Quantum molecular-dynamics study of the electrical and optical properties of shocked liquid nitrogen

S. Mazevet, J. D. Kress, and L. A. Collins
Theoretical Division, Los Alamos National Laboratory, Los Alamos, New Mexico 87545

P. Blottiau
CEA, BP12 F91680, Bruyères Le Châtel, France

(Received 28 July 2002; revised manuscript received 13 December 2002; published 6 February 2003)

Using quantum molecular-dynamics simulations, we show that the electrical and optical properties of shocked liquid nitrogen change drastically as the density increases along the principal and second-shock Hugoniots. Initially, a nonmetal molecular fluid at normal conditions, we find that nitrogen becomes a metal for pressures of 60 GPa and higher. This nonmetal-metal transition for fluid nitrogen can be directly associated to the continuous dissociation occurring along the Hugoniots, and is analogous to the high-pressure nonmetal-metal transition observed experimentally for two other homonuclear diatomic fluids, hydrogen and oxygen.

DOI: 10.1103/PhysRevB.67.054201 PACS number(s): 71.15.Pd, 62.50.+p, 61.20.Ja

I. INTRODUCTION

The recent progress of both the theoretical and experimental tools appropriate for the study of matter under extreme conditions has provided new insights into the drastic changes in physical properties for material subjected to large density variations.[1] A particular area of research has emerged with dynamic compression experiments, where a shock wave compresses a sample to several times its initial density. Using this technique, diatomic fluids, such as hydrogen and oxygen, have recently been shocked to pressures in the 100-GPa range (up to 300 GPa for the former).[2,3] For both species, a nonmetal-metal transition was observed when the pressure was raised to, respectively, 140 GPa and 120 GPa (Refs. 3,4) while the transition itself was identified as a Mott transition.[4] In the present paper, we address the issue of a high-pressure nonmetal-metal transition of another simple diatomic fluid, nitrogen, using quantum molecular dynamics (QMD).

Besides being the most stable diatomic molecule, nitrogen forms numerous chemical compounds. This makes the study of its properties under various pressure and temperature conditions of considerable impact on a wide variety of fields[5] fluids, geology, shocks, detonation, and biology. Furthermore, experimental measurements of shocked liquid nitrogen[6–10] indicate that this molecular system exhibits several features such as the softening of the principal Hugoniot as the density increases, small values of the Gruneisen parameter, and only small increases in temperature when the material is reshocked. We have recently demonstrated that QMD provides a sound description of the equation of state of fluid nitrogen along the principal and second-shock Hugoniots[11,12] based on the overall agreement with the experimental gas gun results. Principal Hugoniot points are the density-pressure (and energy) points reached when the shock wave crosses the media while the second-shock Hugoniots occur experimentally when the shock wave bounces back across the sample for the second time. We also confirmed that most of the features observed experimentally could be related to the continuous dissociation of molecular nitrogen as the increasing pressure breaks the molecular bond.[11,12]

Since QMD simulations combined with the Kubo-Greenwood formulation provide a consistent set of material, electrical, and optical properties from the same simulation,[13] we turn (in the present work), to the electrical and optical properties of shocked liquid nitrogen. We calculate these properties along the principal Hugoniot, where both the density and temperature increase, and along the second-shock Hugoniots, where the density steadily increases while the temperature remains nearly constant along the dissociation region. The latter situation stresses the influence of increasing pressure and minimum temperature variation on the electrical and optical properties of fluid nitrogen.

II. THEORETICAL METHOD

We briefly review some of the main points of our simulations approach; more details appear in earlier publications.[11–13] The frequency-dependent conductivity $\sigma(\omega)$ has both real and imaginary parts:

$$\sigma(\omega)=\sigma_1(\omega)+i\sigma_2(\omega). \tag{1}$$

The real part is derived from the Kubo-Greenwood formulation[14–16]

$$\sigma_1(\omega)=\frac{2\pi}{\Omega\omega}\sum_{i=1}^{ns}\sum_{j=1}^{ns}F_{ij}|D_{ij}|^2\delta(\epsilon_j-\epsilon_i-\omega), \tag{2}$$

where Ω is the atomic volume, ω the frequency, and ns the total number of bands used. F_{ij} stands for the difference between the Fermi-Dirac distributions at temperature T while $|D_{ij}|^2$ represents the velocity dipole matrix element obtained using the ith and jth wave functions found from the diagonalization of the Kohn-Sham equations. To evaluate Eq. (2), we used a Gaussian broadening of the δ functions as described in Ref. 17. The width of the Gaussian is adjusted at each density to be the smallest value that allows the removal of the oscillations in the optical conductivity resulting from

the discrete band structure. For the case of nitrogen presented here, the width of the Gaussian used is typically on the order of 1 eV.

Other properties follow directly from the knowledge of the frequency-dependent real part of the conductivity.[16] The imaginary part arises from the application of a Kramers-Kronig relation as

$$\sigma_2(\omega) = -\frac{2}{\pi} P \int \frac{\sigma_1(\nu)\omega}{(\nu^2-\omega^2)} d\nu, \tag{3}$$

where P stands for the principal value of the integral. The dielectric functions then follow immediately from the two parts of the conductivity:

$$\epsilon_1(\omega) = 1 - \frac{4\pi}{\omega}\sigma_2(\omega), \tag{4}$$

$$\epsilon_2(\omega) = \frac{4\pi}{\omega}\sigma_1(\omega). \tag{5}$$

The real $n(\omega)$ and imaginary $k(\omega)$ parts of the index of refraction are, in turn, related to the dielectric function by a simple formula:

$$\epsilon(\omega) = \epsilon_1(\omega) + i\epsilon_2(\omega) = [n(\omega) + ik(\omega)]^2, \tag{6}$$

or

$$n(\omega) = \sqrt{\frac{1}{2}[|\epsilon(\omega)| + \epsilon_1(\omega)]}, \tag{7}$$

$$k(\omega) = \sqrt{\frac{1}{2}[|\epsilon(\omega)| - \epsilon_1(\omega)]}. \tag{8}$$

Finally, from these quantities, the reflectivity $r(\omega)$ and absorption coefficient $\alpha(\omega)$ are defined as

$$r(\omega) = \frac{[1-n(\omega)]^2 + k(\omega)^2}{[1+n(\omega)]^2 + k(\omega)^2}, \tag{9}$$

$$\alpha(\omega) = \frac{4\pi}{n(\omega)c}\sigma_1(\omega). \tag{10}$$

The latter quantity gives the length absorption or extinction.

The above formulas apply to a spatial configuration of N atoms at a single time step within an MD trajectory. We calculate a trajectory-averaged optical property as

$$\chi = \frac{1}{n_{snap}} \sum_{r=1}^{n_{snap}} \chi_r, \tag{11}$$

where χ_r depicts a representative optical property calculated for a selected configuration r from the MD simulation and n_{snap} is the number of representative configurations or snapshots employed. The configurations, typically five in the present calculations, are spaced at time steps separated by at least the correlation time, the e-folding time of the velocity autocorrelation function.

In the present formulation of QMD, the molecular-dynamics trajectories were calculated using the VASP plane-wave pseudopotential code that was developed at the Technical University of Vienna.[18] This code implements the Vanderbilt ultrasoft pseudopotential scheme[19] in a form supplied by Kresse and Hafner[20] and the Perdew-Wang 91 parametrization of the generalized gradient approximation (GGA).[21]

Trajectories were calculated at fixed volume and at separate density and temperature points, selected to span a range of densities from $\rho = 1.50$ to 4.0 g/cm^3, and temperatures from $T = 1000$ K to $20\,000$ K to highlight the first- and second-shock Hugoniot regions. We used 32 nitrogen atoms in the unit cell and fixed the plane-wave cutoff at 435 eV. Integration of the equations of motion proceeded with time steps of 2 fs. We employ both microcanonical and isokinetic ensembles for the ions. In the latter, the ion temperature T_i is fixed using velocity scaling. In turn, the assumption of local thermodynamical equilibrium sets the electron temperature T_e to that of the ions, T_i. We further point that the method is based on the diagonalization of the electronic Hamiltonian where the electron finite temperature is taken into account by a Fermi smearing over these states. Consequently, the method goes beyond a propagation of the ions on the ground-state Born-Oppenheimer surface. Additional details on the trajectory calculations can be found in Refs. 11,12.

For each snapshot in a given trajectory, the dipole matrix elements $|D_{ij}|^2$ are evaluated using the projector augmented wave method as supplied by Kresse and co-workers.[22,23] Additional details pertaining to the electrical property calculations can be found in Ref. 17.

III. RESULTS AND DISCUSSION

A. Electrical properties

We display in Fig. 1, the variation of the real part of the frequency-dependent conductivity $\sigma_1(\omega)$ at specific density and temperature points dictated by the choice of the initial conditions and the Rankine-Hugoniot relation. The Rankine-Hugoniot equation

$$(U_1 - U_2) + \frac{1}{2}(V_1 - V_2)(P_1 + P_2) = 0, \tag{12}$$

describes the shock adiabat through a relation between the initial and final volumes, internal energy, and pressure, respectively $[[U_1, V_1, P_1)$ and $(U_2, V_2, P_2)]$. For the principal Hugoniot, we have chosen $P_1 = 0$ GPa. $\rho_1 = 0.88$ g/cm^3 in accordance to the experimental conditions, and U_1 so that the energy of the N_2 molecule is zero. The second-shock Hugoniot points are defined similarly, but this time using the final conditions of the first shock as initial conditions. Each experimental point in this case corresponds to a separate second-shock Hugoniot depending on the initial starting point from the principal Hugoniot. Across the dissociation region, the second-shock Hugoniots lie in a fairly narrow temperature band as the pressure increases with density. Therefore, in this regime, an isotherm gives a very good approximation to the second-shock Hugoniot. We select as a

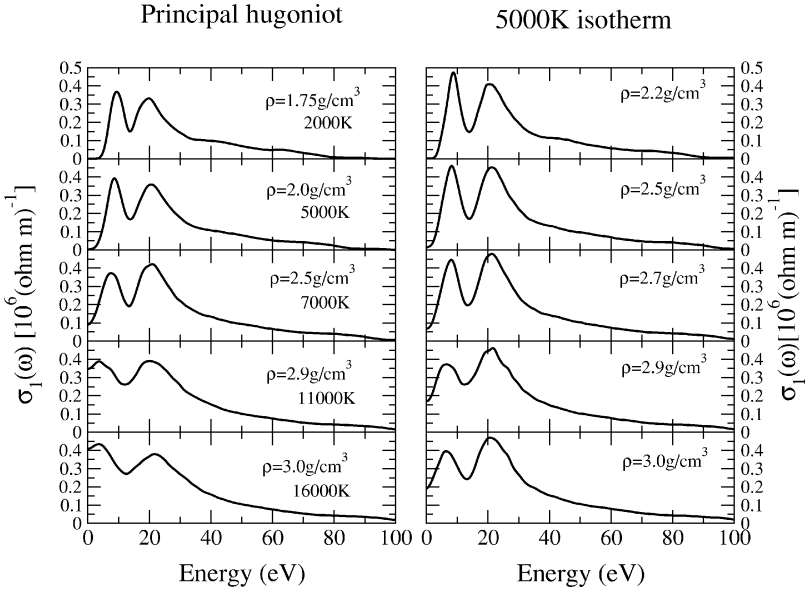

FIG. 1. Variation of the real part of the frequency-dependent conductivity $\sigma_1(\omega)$ along the principal Hugoniot and 5000 K isotherm, respectively (left and right panels).

representative case the isotherm at 5000 K, which corresponds to a final first-shock density of 2 g/cm^3.

For the principal Hugoniot (left panels in Fig. 1), $\sigma_1(\omega)$ was calculated at the temperature closest to the Hugoniot point at which an actual simulation was performed. For the second-shock Hugoniot (right panel in Fig. 1), as the temperature can be considered as constant along the dissociation region,[12] $\sigma_1(\omega)$ was calculated at various densities along the 5000 K isotherm. Calculation of $\sigma_1(\omega)$ as given by Eq.(2) typically involved 700 states, which insured adequate convergence over the frequency range diplayed in Fig. 1.[13] This number of states reflects in the usual sum rule $\int_0^\infty \sigma(\omega)d\omega = \pi e^2 N_e/2m\Omega$, where N_e is the number of electrons in the supercell volume Ω, being satisfied to within 15%. As the latter relation converges slower than the dc and low-frequency ac conductivity, to increase the number of states further would only improve our results for photon energies around 60 eV and higher.[13]

Figure 1 shows that for the lowest density and temperature considered for both the principal and second-shock Hugoniots, the fluid is an insulator. At these conditions, the dc conductivity, given as

$$\sigma_{dc} = \lim_{\omega \to 0} \sigma_1(\omega), \tag{13}$$

is zero. The maximum around 10 eV can be associated with transitions to the lowest excited singlet states of gas-phase molecular nitrogen (N_2). The excited states for molecular nitrogen determined by the density functional approach at the GGA level compare well with experiment. As an example, we find the first singlet excited states at energies of 8.12 eV, 9.711 eV, and 11.70 eV, while the experimental sequence is given by 8.40 eV, 8.55 eV, and 12.93 eV. The first peak at 10 eV in Fig. 1 corresponds to the spread of these excited states due to density effects.

As density and temperature increase along the principal Hugoniot, the frequency-dependent conductivity mostly keeps the same shape but with the first maximum moving to lower frequencies. This results in a significant increase of the dc conductivity that reaches values of around 0.3–0.4 $\times 10^6 \Omega^{-1}\,\mathrm{m}^{-1}$ for the highest density shown.

Inspection of Fig. 1 also indicates that this behavior pertains along the second-shock Hugoniot where the temperature can be considered as almost constant for the density range displayed. Both experimental and QMD results indicate a small temperature variation along the second-shock Hugoniot, i.e., when the material is reshocked.[12] This unique feature of shocked liquid nitrogen also provides the opportunity to probe experimentally the effect of increasing pressure on the nitrogen dc conductivity while keeping the temperature variation to a minimum. To generate experimental states in which the pressure substantially increases without the associated large variation in temperature is the motivation behind the multiple-shock or ''ringup'' experiments performed to measure high-pressure dc conductivity of hydrogen, nitrogen, and oxygen.[1,3,4,24]

The significant variation of the calculated conductivity along the principal and second-shock Hugoniots is highlighted in Fig. 2(a) where the dc conductivities are displayed as a function of pressure. The dc conductivity is negligible along the first Hugoniot ($\sigma_{dc} < 0.1 \times 10^6 \Omega^{-1}\,\mathrm{m}^{-1}$) for pressures up to 40 GPa, rapidly increases up to 0.35 $\times 10^6 \Omega^{-1}\,\mathrm{m}^{-1}$ for pressures between 50 and 60 GPa, after which a mostly constant behavior emerges. Following the evolution of the dc conductivity along the second-shock Hugoniot (5000 K isotherm) shows that a similar behavior results even when the temperature variation is minimal. We noticed however that the increase in dc conductivity shifts to higher values of pressure. Along the second-shock Hugoniot, the dc conductivity becomes significant for pressure values greater than 60 GPa.

In Fig. 2(b), we compare our calculations of the conductivity along the principal Hugoniot and 5000 K isotherm with the currently available experimental data for nitrogen. We see in Fig. 2(b) that the experiments[8,9] also show a distinct rise in the dc electrical conductivity in this critical regime when measured along the principal Hugoniot. The magnitude

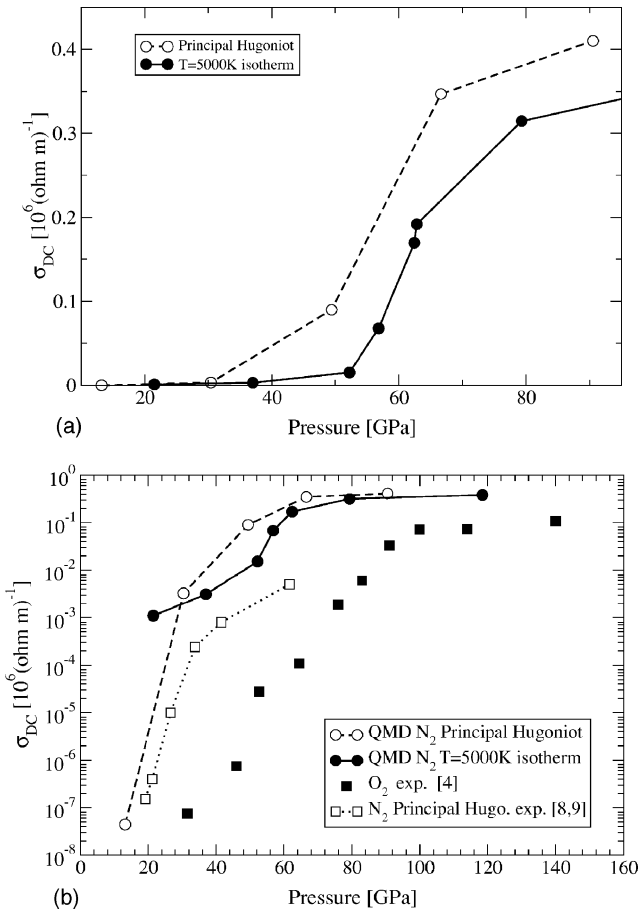

FIG. 2. (a) DC conductivity σ_{dc} as a function of pressure along the principal Hugoniot and 5000 K isotherm. (b) Comparison of the QMD dc conductivities with experimental results.

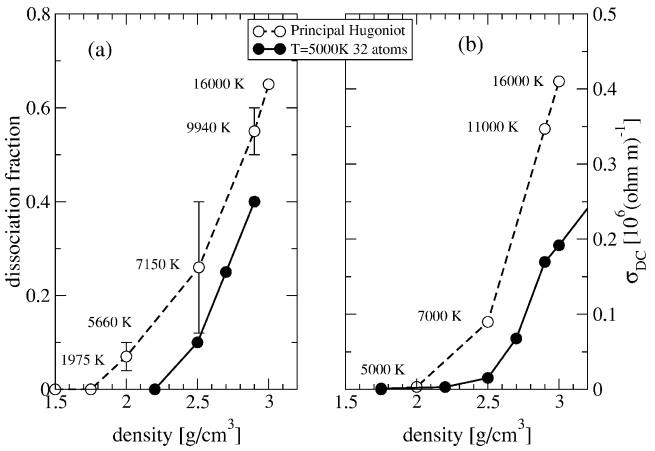

FIG. 3. (a) Dissociation fraction along the first and 5000 K isotherm. (b) Corresponding dc conductivity σ_{dc} as a function of density along the principal Hugoniot and 5000 K isotherm.

of $0.50\times10^4\Omega^{-1}\,\mathrm{m}^{-1}$ at their final point of 60 GPa remains considerably lower than the QMD result of $\sim0.12\times10^6\Omega^{-1}\,\mathrm{m}^{-1}$. However, it should first be pointed out that σ_{dc} exhibits considerable sensitivity to the pressure in this region with a variation spanning almost seven orders of magnitude along the principal Hugoniot. Furthermore, the Gaussian broadening used in the present work brings the largest uncertainties when the conductivity is small. The uncertainties on the evaluation of the conductivity have been estimated at up to a factor of 2 for the smallest pressure points, but reduces to about 10% at the highest pressure point calculated. A slight shift in the onset of this rapid increase in σ_{dc} would also improve the agreement between the experiment and simulations. We have witnessed a similar situation in comparing to the shock reverberation experiments in hydrogen.[25]

Having the experimental conductivities for pressures above 60 GPa would most probably elucidate some of the current discrepancies. Measurements from multiple-shock (reverberation) experiments[4] have been reported for a similar diatomic fluid, oxygen. In Fig. 2(b), we compare the conductivity calculated for nitrogen along the principal Hugoniot and the 5000 K isotherm with the multiple-shock experimental measurements for oxygen.[4] (Similar measurements have already been made for nitrogen, but have not yet been released in quantitative form.[24]) To follow the variation of the nitrogen conductivity above 60 GPa, the limit of the second shock, into the regime of the reverberation experiments, we must extend the 5000 K isotherm to higher densities and pressures. This seems an acceptable procedure since the temperature in the reverberation experiments also remains relatively constant through the compression. In Fig. 2(b), we first notice that the conductivity for the nitrogen principal Hugoniot rises quickly, by about four orders or magnitude (experiment) and six orders of magnitude (calculation) between 20 and 60 GPa. For pressures higher than about 60 GPa, the conductivity for nitrogen reaches a plateau (maximum) for both the principal Hugoniot and 5000 K isotherm. The value of the maximum is in qualitative agreement with the maximum value measured in the oxygen experiment. Since the measured nitrogen conductivity is comparable to the oxygen values for pressures in the 100-GPa range,[24] Fig. 2(b) further shows that the disagreement between our calculations and currently available measurements is in the precise description of the rise in conductivity as the pressure increases rather than in the magnitude of the maximum of the nitrogen conductivity. This rise is very sensitive to temperature along the shock trajectory; as discussed next, the mechanism of the conductivity is related to the dissociation of the molecules. With the multiple-shock technique, higher pressures can be achieved at relatively lower temperatures. For example, in the oxygen experiment, the temperature ranges from 3900 K for $P=100$ GPa to below 7000 K for a pressure up to 200 GPa, whereas in the principal Hugoniot calculations the temperature goes up to 16 000 K [Fig. 3(a)] at a pressure of 90 GPa.

To understand the mechanism giving rise to such a behavior, it is useful to follow the nature of the fluid as the density, temperature, and pressure vary along the principal and second-shock Hugoniots. We show in Fig. 3(a) the variation of the dissociation fraction as a function of density along the principal and second-shock Hugoniots. The dissociation fraction represents the percentage of monomers constituting the fluid. From the simulation, it is obtained by performing a cluster analysis[12] of the MD trajectories. This procedure in-

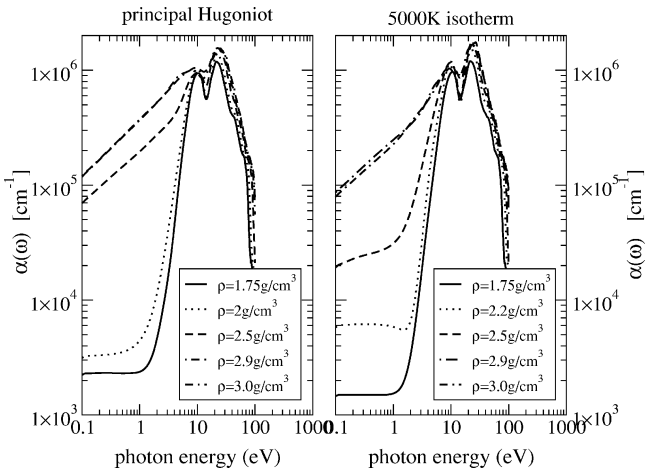

FIG. 4. Variation of the frequency-dependent absorption coefficients $\alpha(\omega)$ along the principal Hugoniot and 5000 K isotherm.

volves selecting an effective radius, in the present case $r_c = 2.3a_B$, and considering all atoms within this distance as bound to a reference atom.[11,12] The distribution of monomers, dimers, and larger molecules obtained at each time step is subsequently averaged over the whole trajectory. The principal Hugoniot dissociation fraction shown in Fig. 3(a) was calculated at density-temperature points above and below the Hugoniot points where the simulations was performed. The ''error bars'' in Fig. 3(a) represent the sensitivity of the dissociation fraction when calculated at these two density-temperature points.

Figure 3(a) shows that for the principal Hugoniot, the fluid starts to dissociate at a density of 2 g/cm^3 and can be considered as fully dissociated at the highest density shown, $\rho = 3$ g/cm^3. The difference from unity at 3 g/cm^3 stems from the fact that the cluster procedure does not distinguish between dimers and binary collisions, which become more important as the density increases. The dissociation fraction, considered in parallel with the lifetime of the dimers and higher-order molecular systems, indicates that at a density of $\rho = 3$ g/cm^3, the fluid is nearly dissociated. Inspection of Fig. 3(b) shows that along the principal Hugoniot, the variation of the dc conductivity as a function of density follows closely the variation of the dissociation fraction with a dissociated molecular fluid showing a conductivity of $\approx 0.4 \times 10^6\ \Omega^{-1}\,\mathrm{m}^{-1}$.

This clearly suggests that the dissociation of the molecular fluid along the Hugoniot has major consequences for the electrical properties of the system. This point is further reinforced when inspecting the second-shock Hugoniot conductivity in conjunction with the corresponding dissociation fraction. The dissociation fraction along the second-shock Hugoniot indicates that as the temperature is kept almost constant, the fluid dissociates when the density increases, but at a density higher than along the principal Hugoniot. We also see that for a given density, as the temperature is lowered, the fluid is systematically less dissociated along the second-shock Hugoniot than along the principal one. This directly reflects the behavior of the second-shock conductivity, which is smaller than that along the principal Hugoniot

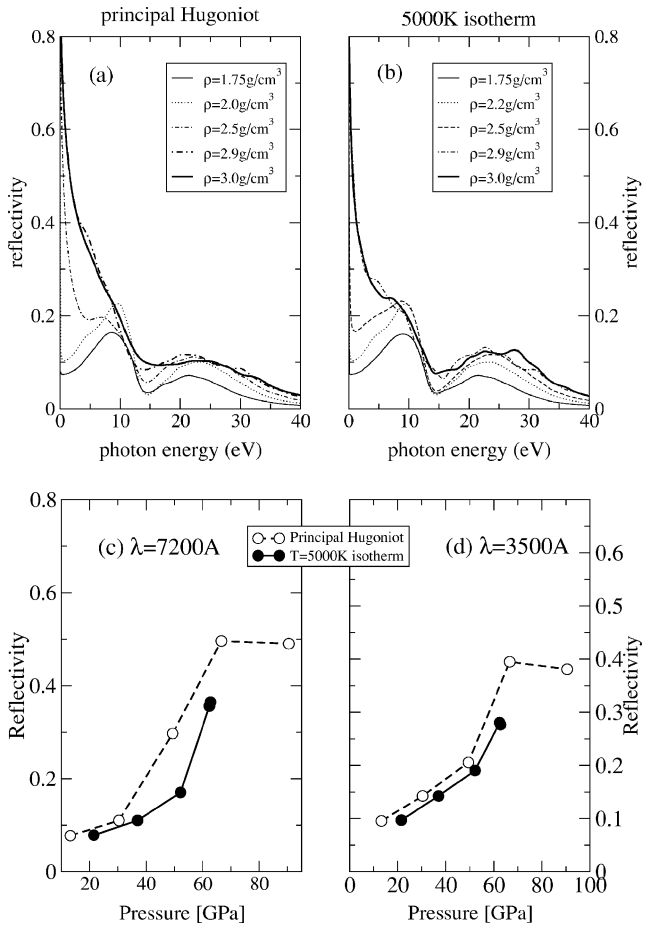

FIG. 5. Variation of the frequency-dependent reflectivity $r(\omega)$ along the (a) principal Hugoniot and (b) 5000 K isotherm. Variation of the reflectivity as a function of pressure at fixed wavelengths of (c) 7200 Å and (d) 3500 Å.

for the density range considered here. This result also suggests that if the density along the second-shock Hugoniot is increased further until the fluid is dissociated, the conductivity will also level at higher pressure as for the principal Hugoniot.

At this stage, it is useful to mention that a similar behavior for the dc conductivity was found experimentally when hydrogen, nitrogen, and oxygen fluids were shocked.[3,4,24] In the case of fluid hydrogen, QMD simulations suggest that the high-pressure nonmetal-metal transition is also closely related to the breaking of molecular bounds as the pressure increases.[13,26] The close connection given above between the behavior of the dc conductivity and the dissociation fraction suggests that, as the molecules dissociate, the resulting atoms (with unpaired electrons) act as dopants, and progressively fill the dense-fluid band gap. For the case of hydrogen, this argument was sustained by calculating the density of states for various temperature-density points corresponding to the experimental measurements.[26] Inspection of Fig. 1, where one sees a progressive filling of the minimum in $\sigma_1(\omega)$ at zero photon energy, suggests that for the case of nitrogen, dissociation is responsible for the high-pressure nonmetal-metal transition.

B. Optical properties

Having shown that a high-pressure nonmetal-metal transition occurs for shocked fluid nitrogen along both the principal and second-shock Hugoniots, we now turn to the implications of such a transition for the optical properties of this system.

In Fig. 4, we display the variation of the absorption coefficient $\alpha(\omega)$ for various density-temperature points along the principal and second Hugoniots. Despite the logarithmic scale, one sees that the variation of the absorption coefficients follows closely the variation of the frequency-dependent conductivity displayed in Fig. 1, as can be expected from Eq. (14). For all the density-temperature points shown, the two maxima around 10 and 20 eV are clearly observed. As mentioned previously, the first maximum can be directly associated with the excited states of molecular nitrogen.

The largest influence of a varying density for the absorption coefficient is seen for photon energies below 10 eV. For example, at a fixed photon energy of 1 eV, the absorption coefficient varies by two orders of magnitude along both the principal and second-shock Hugoniots. We noticed, however, that for either case, this progression is the most dramatic when the fluid starts to dissociate. Following, for example, the progression of the absorption coefficient along the principal Hugoniot shown in Fig. 4(a), we observe the most abrupt increase of the absorption coefficient for densities between 2.0 and 2.5 g/cm^3. As indicated in Fig. 3(a), the fluid just begins to dissociate at those densities. As the density is further increased, the low-photon-energy absorption coefficient stabilizes to values around 1×10^5 cm^{-1} for both the principal and second-shock Hugoniots. This latter point shows that the high-pressure nonmetal-metal transition modifies significantly the optical properties of the shocked fluid.

As dynamic compression experiments have been successful at probing the reflectivity of fluids,[2] we finally show in Fig. 5 the variation of the reflectivity $r(\omega)$ along the principal and second-shock Hugoniots. For both cases, we see little variation of the reflectivity for photon energies higher than 10 eV. As for the absorption coefficients, most of the differences seen in the reflectivity occur at photon energies of 10 eV and lower, with the reflectivity approaching unity asymptotically for zero photon energies as the density is increased along both the principal and second-shock Hugoniots. If we considered typical wavelengths available experimentally, as shown in Figs. 5(c) and 5(d), the high-pressure metal-nonmetal transition will yield a measurable reflectivity increase from 0.1 to 0.4–0.5 for the principal and second shocks. We further point out that, as for the absorption coefficient, the increase in reflectivity mostly ceases once the fluid has started to dissociate, and rapidly reaches a plateau at values less than unity. Such a behavior was also pointed out (both theoretically and experimentally) for the reflectivity of warm, dense hydrogen.[13] As we are finding here for fluid nitrogen, the hydrogen reflectivity rapidly rises and stays constant at values ≈0.5 due to the dissociation of the molecular fluid as the pressure is increased.

IV. CONCLUSIONS

In conclusion, using QMD, we found that a high-pressure nonmetal-metal transition exists for fluid nitrogen. The primary reason for the conductivity increase as the pressure is raised can be traced back to the dissociation of the molecular fluid. As the QMD simulations provide a consistent set of dynamical, electrical, and optical properties from the same simulation, we also calculate the optical properties of warm, dense nitrogen. We associate the high-pressure nonmetal-metal transition with an experimentally measurable increase in the absorption coefficient and reflectivity.

ACKNOWLEDGMENTS

We would like to thank J. D. Johnson, M. Desjarlais, and W. Nellis for helpful discussions. This work was supported under the auspices of the US Department of Energy at Los Alamos National Laboratory under Contract No. W-7405-ENG-36.

[1] R.J. Hemley and N.W. Ashcroft, Phys. Today **51** (8), 26 (1998).
[2] G.W. Collins, L.B. DaSilva, P. Celliers, D.M. Gold, M.E. Foord, R.J. Wallace, A. Ng, S.V. Weber, K.S. Budil, and R. Cauble, Science **281**, 1178 (1998), and references therein.
[3] S. Weir, A.C. Mitchell, and W.J. Nellis, Phys. Rev. Lett. **76**, 1860 (1996).
[4] M. Bastea, A.C. Mitchell, and W.J. Nellis, Phys. Rev. Lett. **86**, 3108 (2001).
[5] P.J. Kortbeekm C.A.T. Seldam, and J.A. Schouten, Mol. Phys. **69**, 1001 (1990); H.D. Jones and F.J. Zerilli, J. Appl. Phys. **69**, 3893 (1991); J. Touret and A.M. van den Kerkhof, Physica B&C **139**, 834 (1986).
[6] R.D. Dick, J. Chem. Phys. **52**, 6021 (1970).
[7] W.J. Nellis and A.C. Mitchell, J. Chem. Phys. **73**, 6137 (1980); W. J Nellis, N.C. Holmes, A.C. Mitchell, and M. van Thiel, Phys. Rev. Lett. **53**, 1661 (1984).
[8] H.B. Radousky, W.J. Nellis, M. Ross, D.C. Hamilton, and A.C. Mitchell, Phys. Rev. Lett. **57**, 2419 (1986).
[9] W.J. Nellis, H.B. Radousky, D.C. Hamilton, A.C. Mitchell, N.C. Holmes, K.B. Christianson, and M. van Thiel, J. Chem. Phys. **94**, 2244 (1991).
[10] G.L. Schott, M.S. Shaw, and J.D. Johnson, J. Chem. Phys. **82**, 4264 (1985).
[11] J.D. Kress, S. Mazevet, L.A. Collins, and W.W. Woods, Phys. Rev. B **63**, 024203 (2001).
[12] S. Mazevet, J.D. Johnson, J.D. Kress, L.A. Collins, and P. Blottiau, Phys. Rev. B **65**, 014204 (2002).
[13] L.A. Collins, S.R. Bickham, J.D. Kress, S. Mazevet, T.J. Lenosky, N.J. Troullier, and W. Windl, Phys. Rev. B **63**, 184110 (2001).
[14] W. A. Harrison, *Solid State Theory* (McGraw-Hill, New York, 1970).

[15] N. W. Ashcroft and N. D. Mermin, *Solid State Physics* (Saunders, Philadelphia, 1976), p. 252.
[16] J. Callaway, *Quantum Theory of the Solid State* (Academic Press, New York, 1974), Sec. 6.5.
[17] M. Desjarlais, J.D. Kress, and L.A. Collins, Phys. Rev. E **66**, 025401 (2002).
[18] G. Kresse and J. Hafner, Phys. Rev. B **47**, 558 (1993); G. Kresse and J. Furthmüller, Comput. Mater. Sci. **6**, 15 (1996); Phys. Rev. B **54**, 11 169 (1996).
[19] D. Vanderbilt, Phys. Rev. B **41**, 7892 (1990).
[20] G. Kresse and J. Hafner, J. Phys.: Condens. Matter **6**, 8245 (1994).
[21] J. P. Perdew, in *Electronic Structure of Solids*, edited by F. Ziesche and H. Eschrig (Akademie-Verlag, Berlin, 1991).
[22] G. Kresse, and J. Joubert, Phys. Rev. B **59**, 1758 (1999).
[23] P.E. Blöchl, Phys. Rev. B **50**, 17 953 (1994).
[24] W. J. Nellis and R. Chau (private communication).
[25] T.J. Lenosky, J.D. Kress, L.A. Collins, and I. Kwon, Phys. Rev. B **55**, R11 907 (1997); L. Collins, J. Kress, S. Bickham, T. Lenosky, and N. Troullier, High Press. Res. **16**, 313 (2000).
[26] T.J. Lenosky, S.R. Bickham, J.D. Kress, and L.A. Collins, Phys. Rev. B **61**, 1 (2000).